Article ID: 1000-324X(2016)01-0100-07 **DOI:** 10.15541/jim20150384

Tribological Behavior of Vacuum Plasma Sprayed B_4C-Mo Composite Coating

LIN Chu-Cheng[1], KONG Ming-Guang[2], ZHU Hui-Ying[3], HUANG Li-Ping[1], ZHENG Xue-Bin[1], ZENG Yi[4]

(1. Key Laboratory of Inorganic Coating Materials, Shanghai Institute of Ceramics, Chinese Academy of Sciences, Shanghai 200050, China; 2. Institute of Solid Physics, Chinese Academy of Scienxes, Hefei 230031, China 3. Biomaterials and Tissue Engineering Research Center, Shanghai Institute of Ceramics, Chinese Academy of Sciences, Shanghai 200050, China; 4. State Key Laboratory of High Performance Ceramics and Superfine Microstructure, Shanghai Institute of Ceramics, Chinese Academy of Sciences, Shanghai 200050, China)

Abstract: A B_4C-Mo composite coating was fabricated using a vacuum plasma spray technique, and its wear behavior was compared with that of a pure B_4C coating. The microstructure of the composite coating was much more homogeneous and compact as a result of the formation of a (B, Mo) C transition phase, which effectively improved the interface between B_4C and Mo splats. For this reason, the wear resistance of the composite coating was much superior to that of the pure B_4C coating. The distribution of nano-sized Mo in the composite coating might also contribute to the improved tribological properties.

Key words: B_4C-Mo composite coating; tribological behavior; vacuum plasma spray

Boron carbide (B_4C) has been a frequent choice as a wear-resistant material owing to its high hardness (55–67 GPa), high melting point (2623 K), and excellent resistance to chemical agents[1-3]. However, the intrinsic brittleness and relatively low sinterability owing to its rigid covalent bonds and low ion diffusion mobility have restricted the widespread application of B_4C as a structural material[4-5]. Instead, many efforts have been made to develop B_4C coatings for structural materials.

Our previous work has already demonstrated that a remarkable improvement in the tribological properties could be obtained by including Ni as a second phase in a vacuum plasma-sprayed B_4C coating[6-7]. Just like Ni, Mo has a remarkably higher thermal conductivity and ductility than B_4C. Therefore, incorporating Mo with the B_4C during deposition could improve heat transfer during spraying, resulting in better cohesion between coating splats. Besides, Mo is known to have excellent wettability for many carbides. According to Wu, *et al*[8], Mo improves the wettability between TiC phase and aluminium melt due to the formation of a Mo-rich shell around the formed TiC particles, which is a kind of good modificator. This supports the idea to prepare B_4C/Mo composite coatings due to the similar performance between TiC and B_4C. Meanwhile, as Kustas, *et al*[9] reports, the addition of Mo to B_4C could significantly reduce the coating damage from complete coating flaking for pure B_4C to a pattern of radial cracks and only partial coating delamination for B_4C-Mo coatings, in which Mo acts as a perfect “binder”. Furthermore, Mo itself is also an outstanding wear-resistant metal that is already widely used in automobile synchronizing rings and piston rings[10]. Moreover, Mo-containing coatings commonly exhibit low coefficients of friction. For example, addition of Mo to aluminum coatings significantly reduces their coefficient of friction[11-12]. Mo alloying of TiN coatings generally enhances their hardness, and the coefficients of friction for TiMoN coatings were found to decrease with increasing Mo atomic fraction when they were tested against a WC-Co pin[13]. Similarly, wear tests of Cr_2O_3-based coatings conducted under dry sliding conditions indicated that the coefficients of friction of Mo-containing coatings were much lower than that of the Mo-free Cr_2O_3 coating[14]. Therefore, the B_4C-Mo composite coating is expected to exhibit excellent wear resistance comparing to the pure B_4C coating.

In present study, a B_4C-Mo composite coating was fabricated by the vacuum plasma spray technique, and its wear behavior was compared with that of the pure B_4C coating. The relationship between tribological properties and the microstructures of the material were also discussed.

Received date: 2015-08-14; **Modified date:** 2015-09-16; **Published online:** 2015-10-30
Foundation items: Open Fund of Key Laboratory of Inorganic Coating Materials, Shanghai Institute of Ceramics, Chinese Academy of Sciences (KLICM-2012-03); Research Project Fund of International Science & Technology Cooperation Project of China (2013DFG52290); Shanghai Technical Platform for Testing and Characterization on Inorganic Materials (14DZ2292900); CAS Key Technolgy Talent Program
Biography: LIN Chu-Cheng(1987–), male, engineer. E-mail: chucheng@mail.sic.ac.cn
Corresponding author: ZENG Yi, professor. E-mail: zengyi@mail.sic.ac.cn

1 Experimental details

1.1 Vacuum plasma spraying of the coatings

Commercially available B_4C (Mudanjiang Jingangzuan Boron Carbide, China) and Mo (Teachn Industrial Technology Development Co., Ltd, Hunan, China) powders with median particle sizes of 30.1 μm and 63.7 μm, respectively, were used. Mixed powders consisting of 85wt% B_4C and 15wt% Mo were ball (ZrO_2) milled for 24 h and then used to fabricate the composite coating.

A vacuum plasma spraying (F4-VB, Sulzer-Metco, Switzerland) system was used to deposit coatings from the initial powders using the optimized spraying parameters listed in Table 1. Before deposition, the stainless steel substrate was cleaned and grit-blasted, and NiCrAlY powder (PR2611, Precursor Plasma Powders, China) was deposited as a bond layer prior to the spraying of the B_4C-Mocomposite coating. A pure B_4C coating was also prepared for comparison.

1.2 Coating characterization and wear testing

The phase composition and morphology of both the feedstock powder and the coatings were identified by X-ray diffraction (XRD, CuKα, λ=1.5406 nm, D/Max-2550V, Rigaku, Japan) and using an scanning electron microscope (SEM, S-4800, Hitachi, Japan) equipped with an energy dispersive spectrometer (EDS, INCA Energy, Oxford, UK), respectively. The microstructures of the coatings were characterized in detail with a transmission electron microscope (TEM, JEM-2100F, JEOL, Japan).

The indentation method (Wilson-Wolpert Tukon2100B, USA) was employed to measure the Vickers microhardness on polished cross sections. Wear tests were performed on a Universal Tribometer Tester (UMT-3, CETR, USA). The tests were conducted at room temperature at a sliding speed of 0.5 m/s. The applied normal loads were 20, 30, 40, and 50 N, with a sliding distance of 900 m. Details of the operation of the system are given elsewhere[7].

2 Results and discussion

2.1 Microstructural characteristics

The XRD patterns of both the pure B_4C coating and the B_4C-Mo composite coating are shown in Fig. 1. Comparing with the pure B_4C coating, the composite coating clearly crystallized well and consisted mainly of the B_4C phase and Mo phase. For plasma spraying process, crystallization of B_4C is not as good as Mo, making the intensity of Mo larger than that of B_4C.

Figure 2 shows the surface and cross-sectional SEM micrographs of as-sprayed coatings. Comparing with the pure B_4C coating (Fig. 2(a)), some fully melted Mo particles were well flattened for the composite coating (Fig. 2(b)), producing a smoother surface. Besides, unlike the pure B_4C coating (Fig. 2(c)), whose cross section was pervaded with spherical pores and angular voids produced by stacking of unmelted splats[6], the B_4C-Mo composite coating exhibited a dense typical lamellar microstructure (Fig. 2(d)) in which Mo (pale region, confirmed by EDS)

Table 1 Vacuum plasma spraying parameters

Parameters	B_4C	B_4C-Mo
Current/A	600	600
Ar gas flow/slpm	37	40
H_2 gas flow/slpm	13	10
Powder feed rate/(r·min^{-1})	22	20
Spray distance/mm	220	200
Pressure/(×10^2, Pa)	400	400
Temperature of the stainless steel substrate/K	520-620	520-620

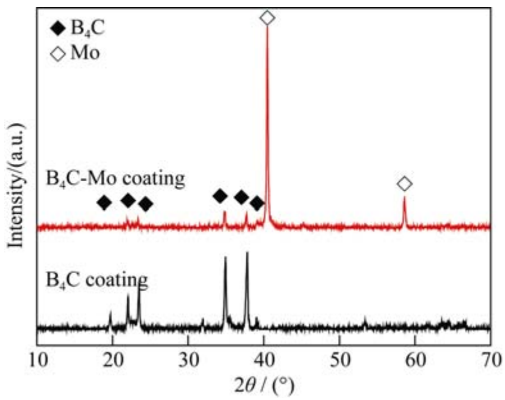

Fig. 1 XRD patterns of as-sprayed coatings

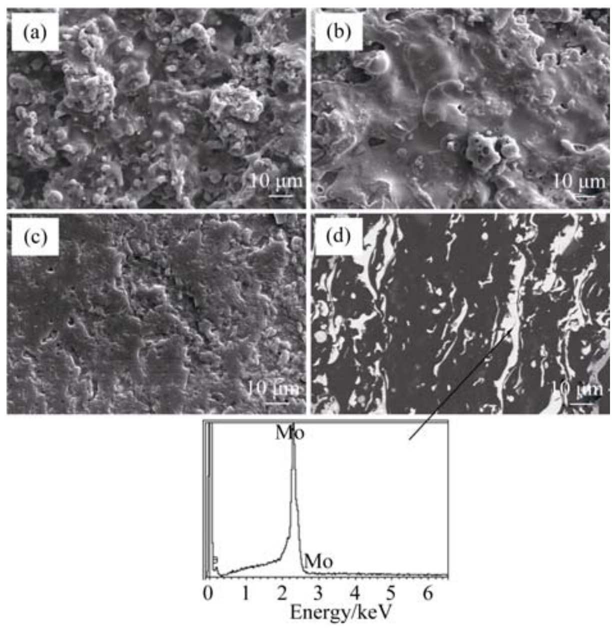

Fig. 2 SEM micrographs of (a, c) B_4C coating and (b, d) B_4C-Mo composite coating; (a, b) surface morphologies and (c, d) cross-sectional morphologies

was distributed homogeneously in the B_4C phase (dark region). This could be attributed to the efficient spreading, overlapping, and filling of Mo droplets in the coating. Since the B_4C-Mo composite coating has a much more desirable microstructure than the pure B_4C coating, its microhardness ((1075±62)HV0.5) is quite close to that of the pure B_4C coating ((1225±190)HV0.5).

Figure 3(a) shows a typical TEM micrograph of a longitudinal section of the B_4C-Mo composite coating. Parallel columnar grains with diameters of approximately 150 nm were observed, and the corresponding EDS analysis verified that they were Mo. Since plasma-sprayed coatings are built up from splats overlapping each other, it is inferred that heat was transported away as soon as the Mo droplet hit the underlying material. Thus, as the droplet spread out, solidification commenced heterogeneously at the interface. Grains nucleated and rapidly grew into the molten splat, forming the columnar grain structure[15–16]. Figure 3(b) shows the distinct morphology of the interface between the B_4C and Mo splats. As can be seen, a well-developed bond was obtained owing to the formation of (B, Mo)C transition phase. This transition phase is quite similar to the Mo-rich shell in sintered materials, which improves the wettability between the ceramic and metallic phases[17-18]. The wettability of the second phase by the matrix obviously has an important influence on the wear performance of the coating[19].

As Fig. 4(a) shows, micro-cracks were visible between particles and splats in the pure B_4C coating. Spherical pores and an amorphous phase are also clearly visible within the splats, illustrating the weak cohesion of the coating, which is believed to arise from stacking faults in the splats, gas entrapment, or lattice mismatches at the interfaces resulting from the discontinuous solidification during plasma spraying. Therefore, a cyclic shear force acting on the B_4C brittle phase during the wear process could lead to crack initiation and propagation, resulting in materials peeling off[20]. The B_4C-Mo composite coating, however, exhibited a much more desirable morphology: the B_4C phase was highly crystallized with easily distinguished grain boundaries, and no obvious defects were found in Fig. 4(b). This was considered to be a result of the Mo second phase. Since the thermal conductivity of the Mo (λ_{Mo}=135 W/(m·K)) is remarkably higher than that of B_4C (λ_{B4C}=17 W/(m·K)), faster heat transfer occurred during spraying, resulting in better cohesion between coating splats.

Meanwhile, because of its thermal expansion coefficient of α_{Mo}=5.75×10^{-6}/K at 1273 K, which is very close to that of B_4C (α_{B4C}=5.73×10^{-6}/K at 300–1970 K)[21-22], the residual thermal stresses resulting from the thermal expansion mismatch in the B_4C-Mo composite coating are expected to be very small.

Figure 4(c)-(f) display typical TEM images showing the morphologies of Mo in the B_4C-Mo composite coating. As

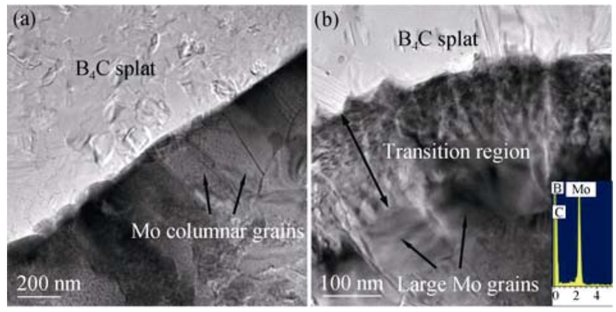

Fig. 3 TEM micrographs of (a) columnar grains and (b) interface between B_4C and Mo splats in the composite coating

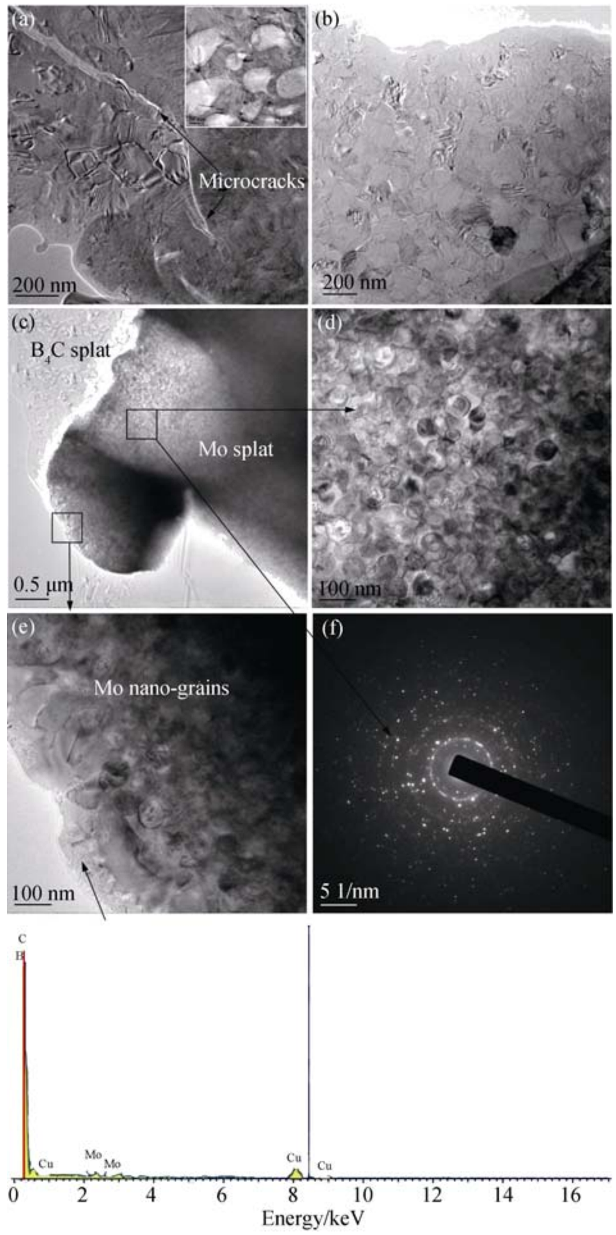

Fig. 4 TEM images showing the different morphologies of the (a) B_4C coating and (b–f) B_4C-Mo composite coating

can be seen, nano-sized Mo grains were formed as a result of the rapid solidification occurring during plasma spraying (Fig. 4(d)-(f)), and the wettability between B_4C and Mo was good, as expected (Fig. 4(e)). The very small grain size of Mo (<100 nm) and the compact interface between B_4C and Mo splats are expected to improve the wear properties.

2.2 Sliding wear behavior

The wear test results for both the B_4C and B_4C-Mo composite coatings are summarized in Fig. 5. As can be seen, the B_4C-Mo composite coating underwent much less material loss and displayed a lower friction coefficient under both low and high load conditions than the pure B_4C coating. In other words, the B_4C-Mo composite coating exhibits superior wear performance.

Figure 6 shows the worn surfaces of the B_4C and B_4C- Mo composite coatings obtained at an applied load of 20 N and sliding speed of 0.5 m/s. Localized flaking pits and micro-fractures can be found on the worn surface of the pure B_4C coating (Fig. 6(a)), indicating that particle pull out and repeated-cycle deformation are the predominant wear mechanisms[10]. The worn surface of the B_4C-Mo composite coating is shown in Fig. 6(b). Material transfer from the counterbody ball to the coating surface clearly occurred during sliding, as verified by the worn scar analysis in Fig. 6(c), and the surface of the composite coating was much more intact than that of the pure B_4C coating after sliding against the WC-Co ball for 1800 s. Despite the appearance of some ploughing grooves parallel to sliding direction, as indicated in Fig. 6(c), nearly no flaking pits or micro-fractures like those observed in the pure B_4C coating were distinguished on the worn surface of the B_4C-Mo composite coating. Thus, the B_4C-Mo composite coating experienced less wear loss. The smoother worn profile of the B_4C-Mo composite coating is probably an indication that plastic deformation happened during the wear test[23], which could alleviate the effect of stress concentration to some degree.

SEM images showing the morphology of the wear debris obtained after the sliding test at 30 N are shown in Fig. 7. As can be seen, the majority of the wear debris for the B_4C coating is flake-like with a relatively large size of hundreds of microns and a thickness of 10–20 μm (Fig. 7(a)). For the B_4C-Mo composite coating, the wear debris gathered was a mixture of flakes and fine particles (Fig. 7(b)), the size of which was no more than 20 μm in length and 5 μm in width.

Figure 8 shows the comparison of surface morphologies of the B_4C-Mo composite coating before and after the wear test under an applied load of 50 N. As Fig. 8(a) and Fig. 8(b) shows, before the wear test, Mo and B_4C were two distinct phases (bright area for Mo and dark area for B_4C), whereas during the wear test, soft and ductile Mo has spread and covered the surface onto B_4C region, since the bright area indicating Mo (Fig. 8(c) and Fig. 8(d)) became evidently larger after the wear test.

2.3 Discussion

The obtained results indicate that the wear resistance of the plasma-sprayed B_4C-Mo composite coating was superior to that of the pure B_4C coating, as shown in Fig. 5 and Fig. 6. The wear behavior of coatings depends on their microstructure, microhardness, friction characteristics, and environmental conditions[24]. As Fig. 2(c) shows, the primary features of the vacuum plasma-sprayed B_4C coating were a large number of scattered cavities and pores. Besides, undesirable micro-cracks and an amorphous phase were also detected in the coating layer (Fig. 4(a)). During wear tests, damage preferentially occurs along preexisting defects such as pores, micro-cracks, or splat interfaces under the elevated cyclic and thermal stress, which results

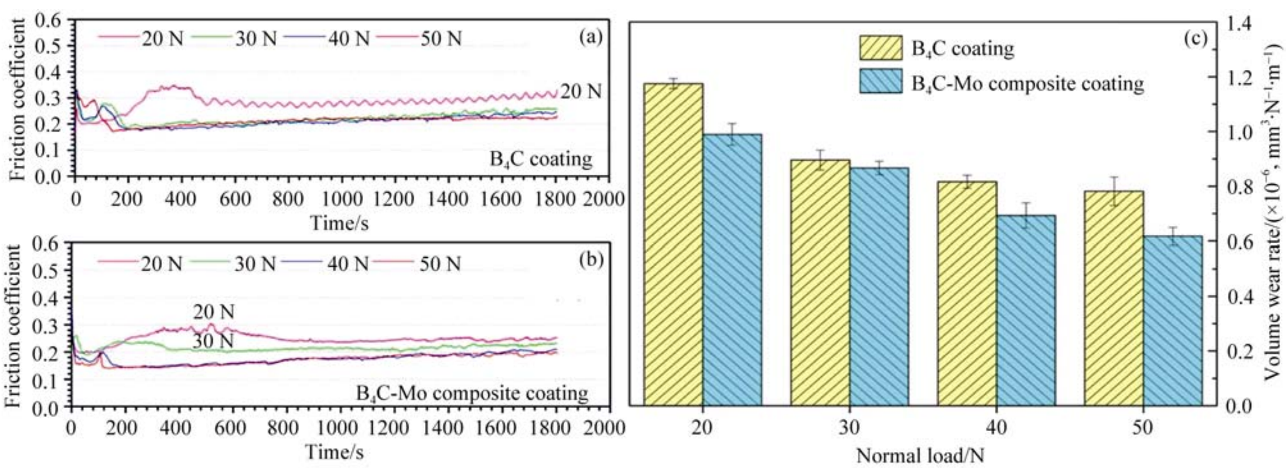

Fig. 5 Friction coefficients depending on sliding time of (a) the B_4C/WC-Co alloy friction pair and (b) the B_4C-Mo/WC-Co alloy friction pair under different loads; (c) comparison of volume wear rates between B_4C and B_4C-Mo composite coatings under different loads

in splat spallation or detachment of the transfer layer[19, 25]. Because of the more compact and homogenous microstructures of the B_4C-Mo composite coating (Fig. 2d), it had superior tribological properties without pits or micro-fractures like those found on the worn surface of the B_4C coating, and the worn surface of the composite coating was maintained almost well (Fig. 6).

A major cause of micro-fracture in ceramics is dislocation pile-up against grain boundaries, which then act as stress concentration sites and trigger grain boundary cracking and grain pull-out. The smaller the grain size, the finer the flaws and the higher the external stress required to induce grain boundary cracking and grain pull-out. The B_4C-Mo composite coating, as shown in Fig. 4(c), contained a large amount of nano-sized Mo grains, which might restrict the crack size, create a large volume of grain boundaries, and hence improve the coating toughness and contact load support[26]. Furthermore, grain boundaries are believed to be one of the areas where absorbed energy is stored. As a result, the larger the boundary volume, the more energy could be absorbed, and therefore finer grain sizes could lead to greater wear resistance of the material (Fig. 5 and Fig. 6).

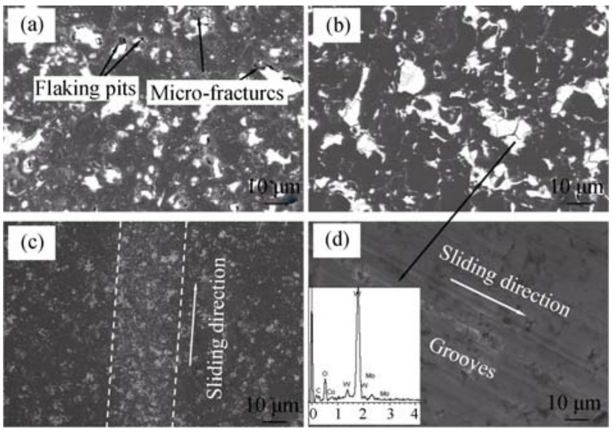

Fig. 6 SEM images showing the morphologies of worn surfaces after sliding against a WC-Co ball for 1800 s with an applied load of 20 N

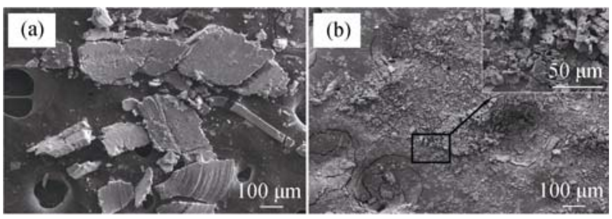

Fig. 7 SEM micrographs of wear debris obtained for (a) B_4C and (b) B_4C-Mo coatings

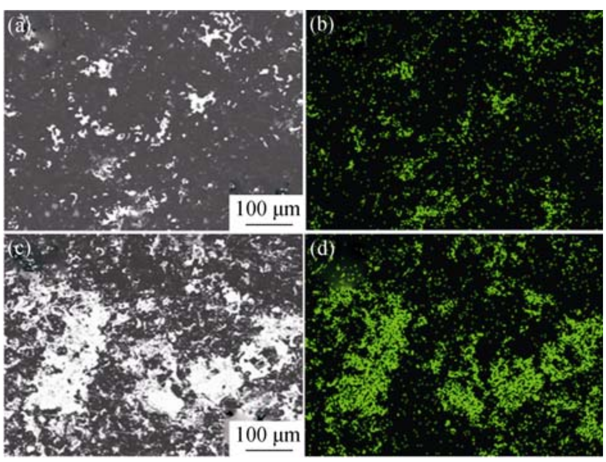

Fig. 8 Comparison of surface morphologies for the B_4C-Mo composite coating (a, b) before and (c, d) after the wear test under an applied load of 50 N; (a, c) SEM micrographs and (b, d) corresponding EDS mapping of Mo

Guo, *et al*[27] reported that the wettability of carbides by Mo and the carbide-Mo interface strength are also important factors that influence the wear performance of coatings. In the sliding wear tests, coatings were subjected alternately to tensile and compression stresses, and cracks would initiate in the subsurface, where the materials suffer the maximum shear stress. When these subsurface cracks propagate through splats or along splat boundaries, material removal occurs. For the B_4C-Mo composite coating, because of the formation of the (B, Mo)C transition phase, the carbide-metal interface strength was notably improved, which effectively prevented the well-adhered splats from cracking. Therefore, after sliding against WC-Co ball for 1800 s, particle pull-out was very limited for the B_4C-Mo composite coating, as illustrated in Fig. 6(b). In summary, the B_4C-Mo composite coating exhibited good coating cohesion and outstanding wear resistance.

Comparison of surface morphologies observed before and after the wear test (Fig. 8) suggests another possible mechanism for the friction reduction of the B_4C-Mo composite coating. During sliding, B_4C was the dominant phase with a high hardness, while Mo was interlaced into the coating structure. As the Mo deformed under the load during the wear test, it smeared on the surface of B_4C. As Fig. 8 indicates, before the wear test, Mo and B_4C were two distinct phases, whereas after the wear test the two phases were merged into one another, and the Mo was more evenly scattered on the wear track. This scattered Mo likely provided the required dry sliding properties for the coating surface. Furthermore, the Mo on the coating surface might also prevent seizure between the coating and the ball[28], leading to a further marginal improvement in the wear performance of B_4C-Mo composite coating.

3 Conclusion

The B_4C-Mo composite coating was successfully fabricated by vacuum plasma spraying, and its microstructure and friction characteristics sliding against WC-Co alloy at room temperature were evaluated. It was found that a transition phase of (B, Mo)C was produced during spraying in the composite coating, which effectively improved the wettability of the carbide phase by Mo and led to stronger bonding at the carbide-metal interface. Because of its more homogenous microstructure, the B_4C-Mo composite coating exhibited both a lower friction coefficient and a lower volume wear rate than the pure B_4C coating, at least for sliding against WC-Co alloy under the conditions used in the present study. The improvement in the wear resistance of the B_4C-Mo composite coating was also attributed to the formation of nano-sized Mo in the composite coating, as well as its higher thermal conductivity.

References:

[1] SALIMIJAZI H R, COYLE T W, MOSTAGHIMI J, *et al*. Microstructure of vacuum plasma-sprayed boron carbide. *Journal of Thermal Spray Technology*, 2005, **14(3):** 362–368.

[2] LEE H, SPEYER R F. Pressureless sintering of boron carbide. *Journal of the American Ceramic Society*, 2003, **86(9):** 1468–1473.

[3] FRANCOIS THEVENOT. Boron carbide - a comprehensive review. *Journal of the European Ceramic Society*, 1990, **6:** 205–225.

[4] YAMADA S, HIRAO K, YAMAUCHI Y, *et al*. High strength B_4C-TiB_2 composites fabricated by reaction hot pressing. *Journal of European Ceramic Society*, 2003, **23(7):** 1123–1130.

[5] SUN J L, LIU C X, DUAN C Y. Effect of Al and TiO_2 on sinterability and mechanical properties of boron carbide. *Materials Science & Engineering A*, 2009, **509(1/2):** 89–93.

[6] ZHU H Y, NIU Y R, LIN C C, *et al*. Fabrication and tribological evaluation of vacuum plasma sprayed B_4C coating. *Journal of Thermal Spray Technology*, 2012, **21(6):** 1216–1223.

[7] ZHU H Y, NIU Y R, LIN C C, *et al*. Microstructures and tribological properties of vacuum plasma sprayed B_4C-Ni composite coatings. *Ceramics International*, 2013, **39(1):** 101–110.

[8] WU Q, YANG C, XUE F, *et al*. Effect of Mo addition on the microstructure and wear resistance of *in situ* TiC/Al composite. *Materials & Design*, 2011, **32(10):** 4999–5003.

[9] KUSTAS F, MISHRA B, ZHOU J. Wear behavior of B_4C- Mo co-sputtered wear coatings. *Surface and Coatings Technology*, 2001, **141(1):** 48–54.

[10] WANG B H, LEE S, AHN J. Correlation of microstructure and wear resistance of molybdenum blend coatings fabricated by atmospheric plasma spraying. *Materials Science & Engineering A*, 2004, **366(1):** 152–163.

[11] ABU-ZEID O A, BATES R I. Friction and corrosion resistance of sputter deposited supersaturated metastable aluminium-molybdenum alloys. *Surface & Coatings Technology*, 1996, **86-87(1/2/3):** 526–529.

[12] BIELAWSKI M. Development of unbalanced magnetron sputtered Al-Mo coatings for cadmium replacement. *Surface & Coatings Technology*, 2004, **179(1):** 10–17.

[13] YANG Q, ZHAO L R, PATNAIK P C, *et al*. Wear resistant TiMoN coatings deposited by magnetron sputtering. *Wear*, 2006, **261(2):** 119–125.

[14] AHN H S, LYO I W, LIM D S. Influence of molybdenum composition in chromium oxide-based coatings on their tribological behavior. *Surface & Coatings Technology*, 2000, **133:** 351–361.

[15] DE ARELLANO-LO´PEZ ANTONIO R, FABER K T. Microstrucutural characterization of small-particle plasma spray coatings. *Journal of the American Ceramic Society*, 1999, **82(8):** 2204–2208.

[16] BENGTSSON P, JOHANNESSON T. Characterization of microstructure defects in plasma sprayed thermal barrier coatings. *Journal of Thermal Spray Technology*, 1995, **4(3):** 245–251.

[17] LI Y, LIU N, ZHANG X, *et al*. Effect of Mo addition on the microstructure and mechanical properties of ultra-fine grade TiC-TiN-WC-Mo_2C-Co cermets. *International Journal of Refractory Metals &Hard Materials*, 2008, **26(3):** 190–196.

[18] CHRASKA T, KING A H. Transmission electron microscopy study of rapid solidification of plasma sprayed zirconia—Part II: interfaces and subsequent splat solidification. *Thin Solid Films*, 2001, **397(1/2):** 40–48.

[19] PSYLLAKI P P, JEANDIN M, PANTELIS D I. Microstructure and wear mechanism of thermal-sprayed alumina coatings. *Materials Letters*, 2001, **47(1/2):** 77–82.

[20] GUILEMANY J M, ARMADA S, MIGUEL J M. Evaluation of wear damage in zirconia plasma-sprayed coatings using scanning white light interferometry. *Journal of Thermal Spray Technology*, 2001, **10(1):** 142–146.

[21] BARTOLOMÉ J F, DÍAZ M, REQUENA J, *et al*. Mullite/ molybdenum ceramic–metal composites. *Acta Materialia*, 1999, **47(14):** 3891–3899.

[22] WANG Y, JIANG S, WANG M D, *et al*. Abrasive wear characteristics of plasma sprayed nanostructured alumina/titania coatings. *Wear*, 2000, **237(2):** 176–185.

[23] XIE Y, HAWTHORNE H M. The damage mechanisms of several plasma-sprayed ceramic coatings in controlled scratching. *Wear*, 1999, **233-235:** 293–305.

[24] UYULGAN B, CETINEL H, OZDEMIR I, *et al*. Friction and wear

properties of Mo coatings on cast-iron substrates. *Surface & Coatings Technology*, 2003, **174-175:** 1082–1088.

[25] VIJANDE-DIAZ R, BELZUNCE J, FERNANDEZ E, *et al*. Wear and microstructure in fine ceramic coatings. *Wear*, 1991, **148(2):** 221–233.

[26] HU J J, MURATORE C, VOEVODIN A A. Silver diffusion and high-temperature lubrication mechanisms of YSZ-Ag-Mo based nanocomposite coatings. *Composites Science and Technology*, 2007, **67(3/4):** 336–347.

[27] GUO X Q, NIU Y R, HUANG L P, *et al*. Microstructure and tribological property of TiC-Mo composite coating prepared by vacuum plasma spraying. *Journal of Thermal Spray Technology*, 2012, **21(5):** 1083–1090.

[28] NIRANATLUMPONG P, KOIPRASERT H. The effect of Mo content in plasma-sprayed Mo-NiCrBSi coating on the tribological behavior. *Surface & Coatings Technology*, 2010, **205(2):** 483–489.

真空等离子体喷涂 B_4C-Mo 复合涂层耐磨性能研究

林初城[1], 孔明光[2], 朱慧颖[3], 黄利平[1], 郑学斌[1], 曾 毅[4]

(1. 中国科学院 上海硅酸盐研究所, 特种无机涂层重点实验室, 上海 200050; 2. 中国科学院 上海硅酸盐研究所, 生物材料与组织工程研究中心, 上海 200050; 3. 中国科学院 固体物理研究所, 合肥 230031; 4. 中国科学院 上海硅酸盐研究所, 高性能陶瓷和超微结构国家重点实验室, 上海 200050)

摘 要: 采用真空等离子体喷涂技术制备了 B_4C-Mo 复合涂层, 并对其耐磨性能进行了研究。与 B_4C 纯涂层相比, 复合涂层结构更为致密, (B, Mo)C 过渡相的存在改善了 B_4C 相与 Mo 相之间的润湿性, 进而有效提高了涂层的抗摩擦磨损性能。此外, Mo 在喷涂过程中形成了大量的纳米晶, 这也在一定程度上促进了复合涂层耐磨性能的提高。

关 键 词: B_4C-Mo 复合涂层; 耐磨性能; 真空等离子体喷涂

中图分类号: TG174 **文献标识码:** A